

# High Power Arcjet

T. M. Gölz, M. Auweter-Kurtz,  
H. L. Kurtz, and H. O. Schrade

Institut für Raumfahrtssysteme  
Stuttgart University  
IRS 92-P4

Fourth Progress Report  
NASA Grant No. NAGW-1736

March 1992

## Abstract

*This fourth Progress Report covers the activities on the High Power Arcjet project from February 1991 to February 1992.*

*In this period a new mass flow controller was brought into the gas supply system, so that the upper limit for the mass flow rate could be increased up to 500 mg/s with hydrogen.*

*A maximum specific impulse of 1500 s could be achieved with HIPARC at an efficiency of slightly better than 20 %. Different nozzle throat diameters had been tested. The 100 kW input power limit was reached with the 4 mm nozzle throat diameter at a mass flow rate of 400 mg/s. Tests were carried out with different cathode gaps and with three different cathodes. In addition measurements of pressure and gas temperature were taken in the feed line in order to determine the pressure drop in the propellant injectors.*

*As the next step in the program is the development of a radiation cooled high power arcjet thruster, the design of this thruster is also presented in this report.*

# Contents

Abstract .....	2
Contents .....	3
Introduction .....	4
Experimental Results .....	4
Measurements of the Feed Line Gas Conditions .....	4
Cathode Gap Variation .....	4
Variation of the Ambient Pressure .....	6
Pressure Distribution in the Thruster/Expansion Ratios .....	8
Radiation Cooled HIPARC Thruster Design .....	10
References .....	12
Appendix A .....	13

## Introduction

Most of the HIPARC data taken have been published at the 22nd International Electric Propulsion Conference, October 1991 in Viareggio, Italy. The paper IEPC-91-072 "High Power Arcjet Thruster Experiments" describes the results obtained until September 1991. This paper is included as Appendix A in this progress report.

Further experimental results obtained in the time after the conference are presented in the section "Experimental Results". The design of the radiation cooled high power arcjet (HIPARC-R) is presented in the last section.

## Experimental Results

### Measurements of the Feed Line Gas Conditions

In order to get informations about the gas conditions in the feed line and the pressure drop in the propellant injectors pressure and temperature were measured in the feed line 70 cm upstream of the injection nozzles. The pressure was measured by a absolute pressure strain gauge of a full scale range of 10 bar. The gas temperature was measured by a thermocouple.

The results of the feed line pressure measurement can be seen in Figs. 8 and 9. The gas temperature in the feed line could not be measured correctly with the thruster operating. Typical pressure/temperature values in the feed line before thruster ignition are 20° C (equals 293 K) and 1850 mbar at 100 mg/s mass flow rate, and 21-22° C and 3600 mbar at 200 mg/s. At the 300 mg/s mass flow rate the pressure is at about 5300 mbar. The measured temperature values of about 11° C (equals 284 K) seem to be too low compared to the other temperature data; disturbances are likely.

### Cathode Gap Variation

In addition to the diagrams presented in the paper, some more figures referring to the cathode gap variation are given below. Figs. 1 and 2 show the variation of arc voltage with the cathode gap. Although there are only three cathode gaps per power level it is obvious that the arc voltage does not vary directly with the electrode gap, but that the increase in voltage gets smaller with longer electrode gaps. This effect is stronger at higher current and power levels.

Previous results with HIPARC (see Appendix A) and with other thrusters [1] show that the larger arc gaps yield higher arc chamber pressures, indicating higher arc chamber temperature values (because the particle density is not influenced by the arc gap). Higher plasma temperatures increase the electric conductivity, so that the voltage drop in the arc gets smaller.

New test runs with the 4 mm nozzle throat diameter were performed with the variation of the cathode gap. Until now only electrode gaps of 3 mm and 4 mm have been tested. As can be seen in Fig. 3 the arc gap has a significant influence on arc chamber pressure, but almost none on specific impulse at constant specific input power (Fig. 4) and thus no influence on thrust efficiency.

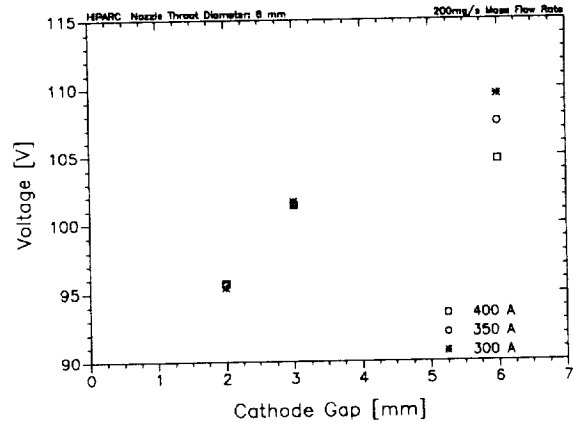
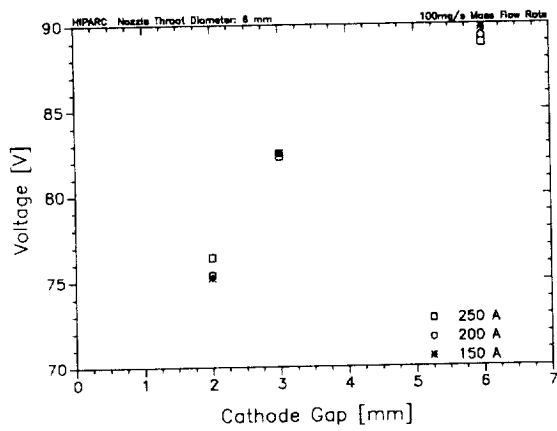


Fig. 1: Arc Voltage versus Cathode Gap at constant arc current. Mass flow rate is 100 mg/s (left) and 200 mg/s (right), respectively.

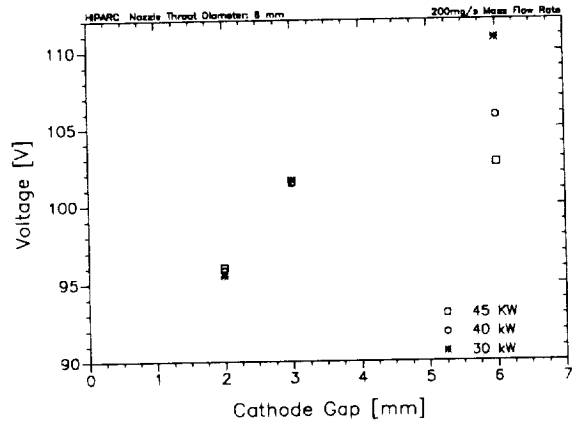
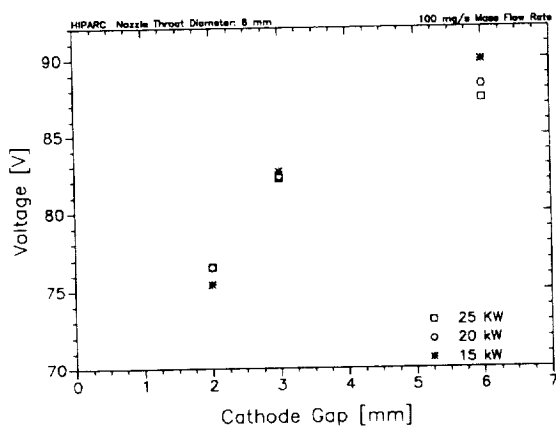


Fig. 2: Arc Voltage versus Cathode Gap at constant input power. Mass flow rate is 100 mg/s (left) and 200 mg/s (right), respectively.

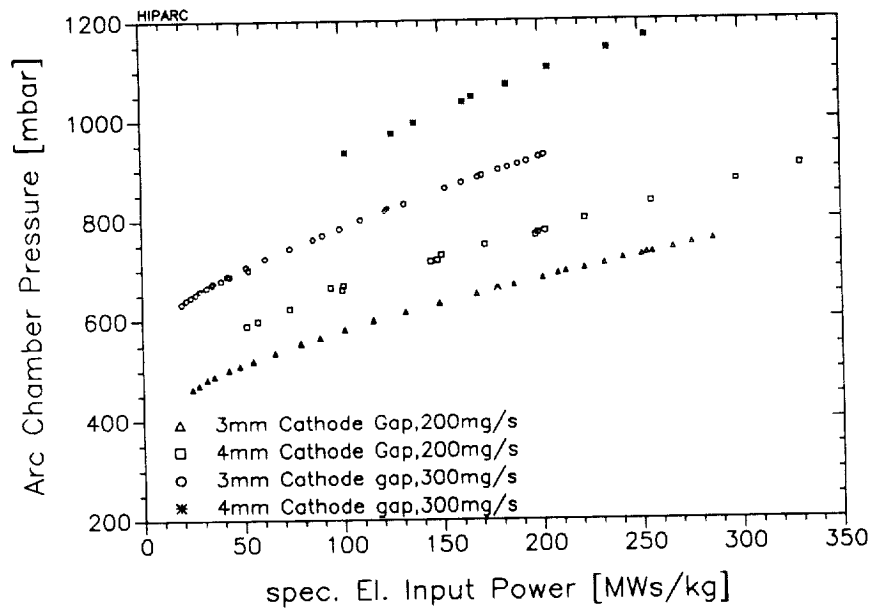


Fig. 3: Arc chamber pressure at two different arc gaps with the 4 mm nozzle throat diameter.

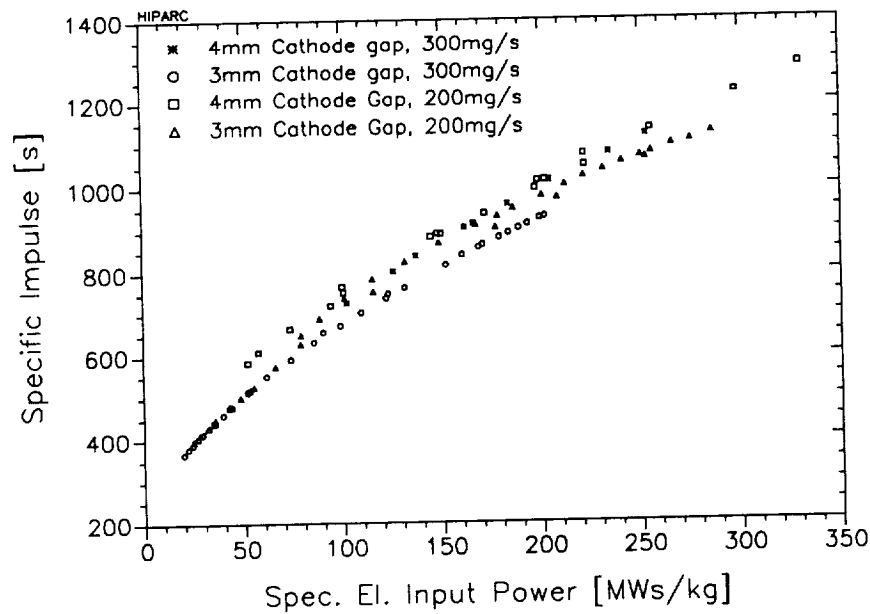


Fig. 4: Thruster performance at two different arc gaps with the 4 mm nozzle throat diameter.

### Variation of the Ambient Pressure

Because it is of importance to know how such a thruster performs in space the simulation of space vacuum is necessary. As the ambient pressure possible with our vacuum system does not space vacuum levels, it is attempted to investigate the influence of the ambient pressure in order to forecast thruster space performance. The ambient pressure levels were varied by adding an ALCATEL roots pump to the vacuum system, which lowers the ambient pressure by increasing the suction capacity, so that the biggest effect can be observed at high mass flow rates. Fig. 5 shows both ambient pressure levels, with and without the additional pump in operation, versus the specific input power. The characteristic shows a decreasing ambient pressure with increasing input power in both cases. This is due to the diffuser effect that increases with increasing plasma velocity. The rapid growth of the background pressure at the 300 mg/s low pressure level test was due to a failure in the vacuum system that resulted in a thruster shut-down.

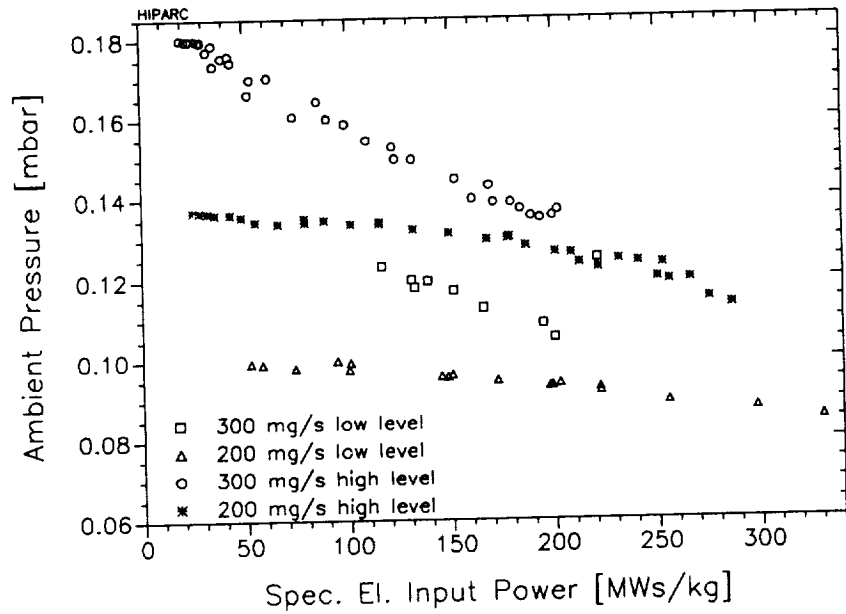


Fig. 5: Ambient Pressure Levels with and without additional pump.

The results show a better thruster performance at the low ambient pressure level, which is mainly because of the force resulting from the product of pressure difference and nozzle exit area. Exact values are given in Table 1 below.

$P_{spec}$ [MJ/kg]	$F_{P_{high}}$ [N]	$F_{P_{low}}$ [N]	$\Delta F$ [N]	$\Delta p$ [mbar]	$\Delta F_p$ [N]
100	1.452	1.477	0.025	0.034	0.011
150	1.708	1.748	0.040	0.035	0.012
200	1.924	1.955	0.031	0.033	0.011

Tab. 1: Comparison between thrust differences at different ambient tank pressures.

The changes in thrust are within the accuracy ( $\pm 0.04$  N, see [3]) of the thrust measurement. Other test runs have to be made with higher mass flow rates, where higher pressure and thus thrust differences are expected.

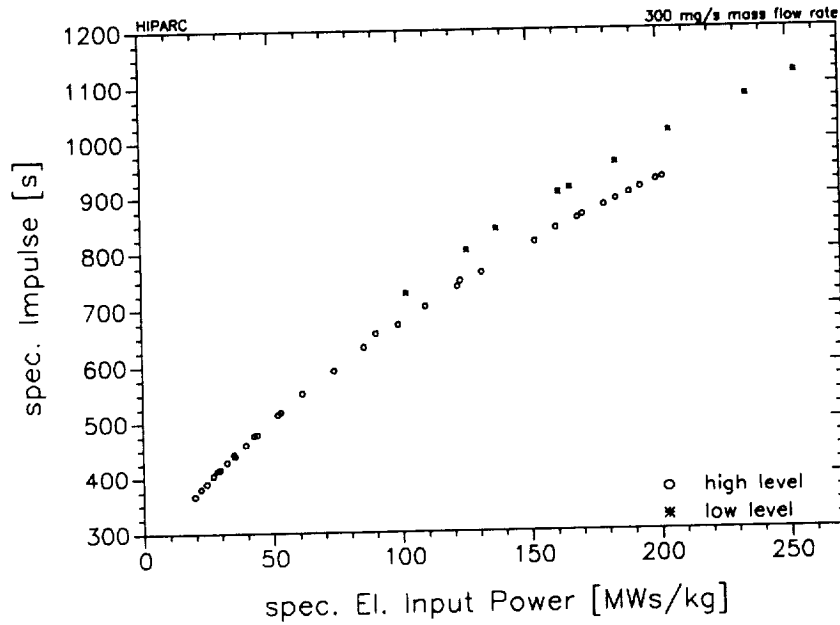


Fig. 6: Influence of the Ambient Pressure on Specific Impulse at a mass flow rate of 300 mg/s.

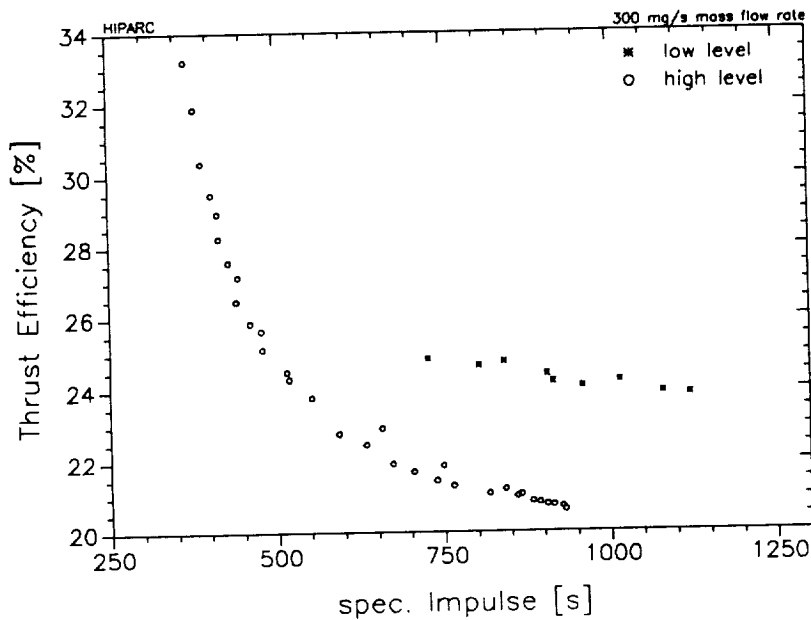


Fig. 7: Influence of the Ambient Pressure on Thrust Efficiency at a mass flow rate of 300 mg/s.

### Pressure Distribution in the Thruster/Expansion Ratios

Measurement of the arc chamber pressure is almost impossible with radiation cooled thrusters. This is why most authors measure the feed line pressure instead. In order to be able to determine the feed line pressure from the arc chamber pressure test runs were made where the feed line, the arc chamber, and the ambient tank pressure data was taken. The Figures below (Figs. 8 and 9) show the pressure distributions in the thruster for the 200 mg/s and for the 300 mg/s mass flow rate. The results are obtained with four injection nozzles with a 0.6 mm bore hole diameter.



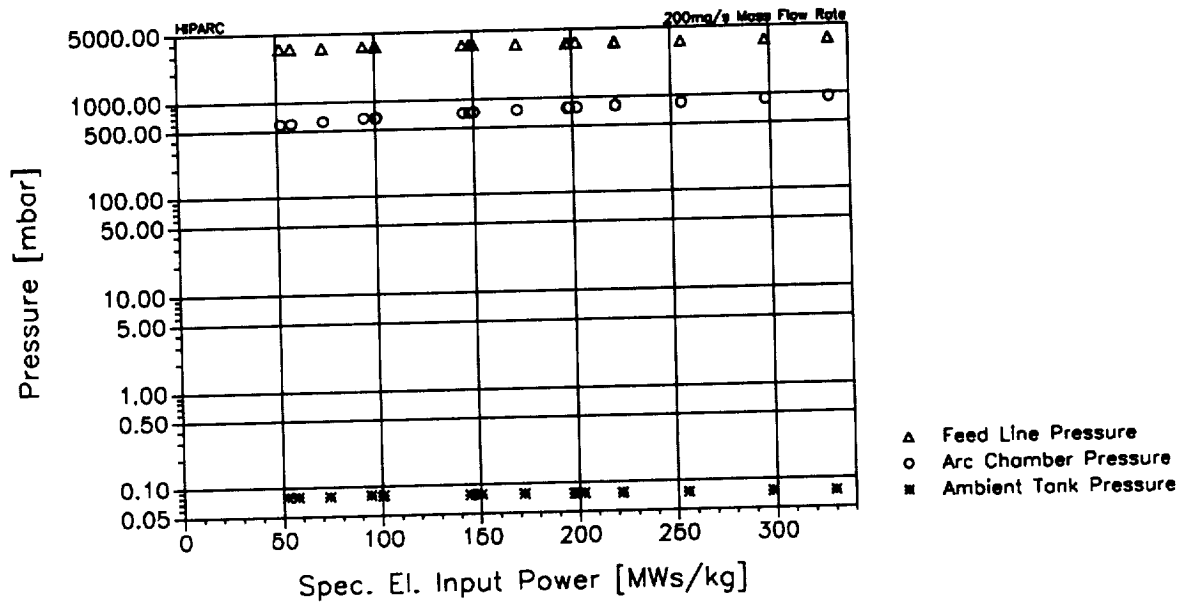


Fig. 8: Pressure Distribution in the Thruster at a 200 mg/s Mass Flow Rate.

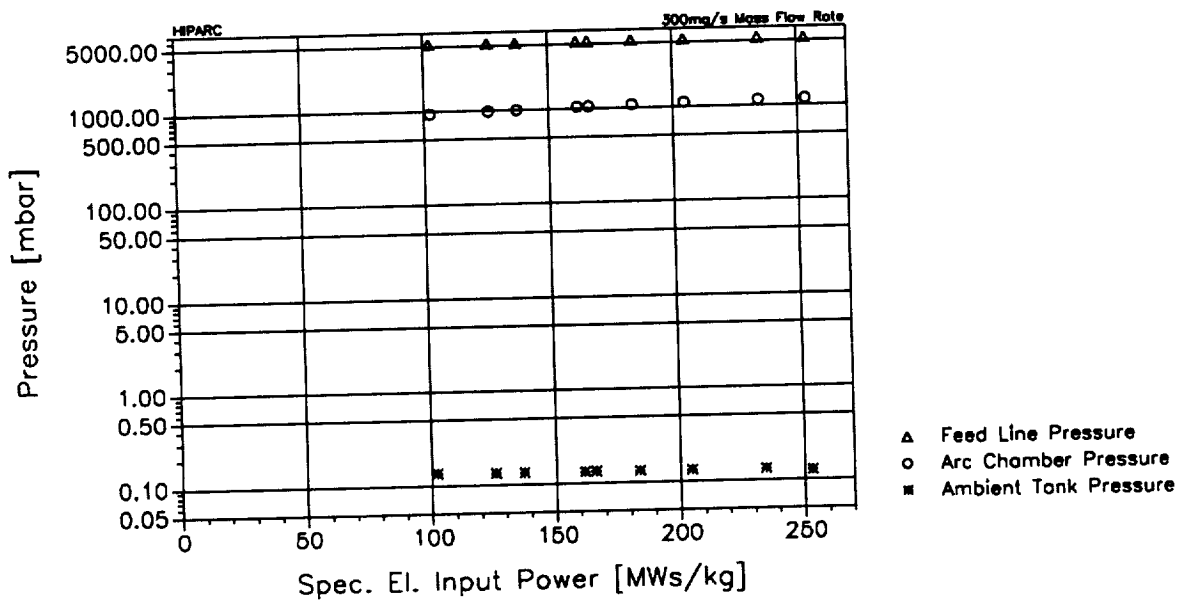


Fig. 9: Pressure Distribution in the Thruster at a 300 mg/s Mass Flow Rate.

The pressure distributions yield expansion ratios as listed in the following tables (Tabs. 2 and 3). The injector nozzle expansion ratio lies between 5.6 and 4.0, varying inversely with the specific input power. As the nozzle end pressure was not measured, the expansion ratio  $\epsilon_{\text{nozzle}}$  (which is arc chamber pressure divided by the ambient tank pressure) is an approximation of the nozzle expansion ratio value. Herein the ambient tank pressure was assumed to be equal to the nozzle end pressure.

$P_{spec}$ [MJ/kg]	$P_{fl}$ [mbar]	$P_c$ [mbar]	$P_{tank}$ [mbar]	$\epsilon_{injector}$ [-]	$\epsilon_{nozzle}$ [-]
100.7	3641.	669.	7.97E-2	5.45	8388
150.2	3610.	728.	7.78E-2	4.96	9357
197.5	3592.	767.	7.63E-2	4.68	10059
255.3	3609.	834.	7.47E-2	4.33	11170
298.0	3633.	877.	7.38E-2	4.14	11886
329.9	3643.	907.	7.31E-2	4.02	12397

Tab. 2: Expansion Ratio at the 200 mg/s mass flow rate.

$P_{spec}$ [MJ/kg]	$P_{fl}$ [mbar]	$P_c$ [mbar]	$P_{tank}$ [mbar]	$\epsilon_{injector}$ [-]	$\epsilon_{nozzle}$ [-]
102.2	5259.	935.	0.134	5.62	6979
161.6	5293.	1036.	0.131	5.11	7936
204.6	5359.	1105.	0.131	4.85	8461
253.2	5366.	1168.	0.125	4.59	9320

Tab. 3: Expansion Ratios at the 300 mg/s mass flow rate.

## Radiation Cooled HIPARC Thruster Design

The development of a radiation cooled high power arcjet thruster has begun in December 1991 and led to the design presented here. The overall dimensions have been chosen according to temperature measurements with the Institute's radiation cooled 10 kW arcjet thruster and finite element thermal calculations performed with this 10 kW thruster geometry [1]. In addition a scale-up of the results from radiative heat flux measurements taken by *Sankovic and Curran* [2] had been used to check the design.

Fig. 10 shows a cross sectional and a front view of this thruster. The most obvious feature is the technique the nozzle is fastened to the thruster housing. In order to keep the housing as small as possible a cramping technique is used to fix the anode onto the housing. The nozzle is centered by the injector disk.

The thruster dimensions were determined under the following assumptions:

1. A portion of 10 % of the electric input power have to be radiated off the housing.
2. The emission coefficient is  $\epsilon = 0.4$ .
3. The anode temperature must not exceed 2300 K.

These assumptions yields a nozzle surface area required of 157.6 cm<sup>2</sup>, which is a 7.2 cm nozzle length at a diameter of 7 cm. The anode loss of 10 % of the total input electrical power was taken from *Sankovic and Curran* [2], where anode loss rates of between 8 % and 15 % had been measured with the hydrogen operated radiation cooled device at higher mass flow rate and input power levels. Besides that we still have the option to increase the emissivity of the nozzle material by coating the body.

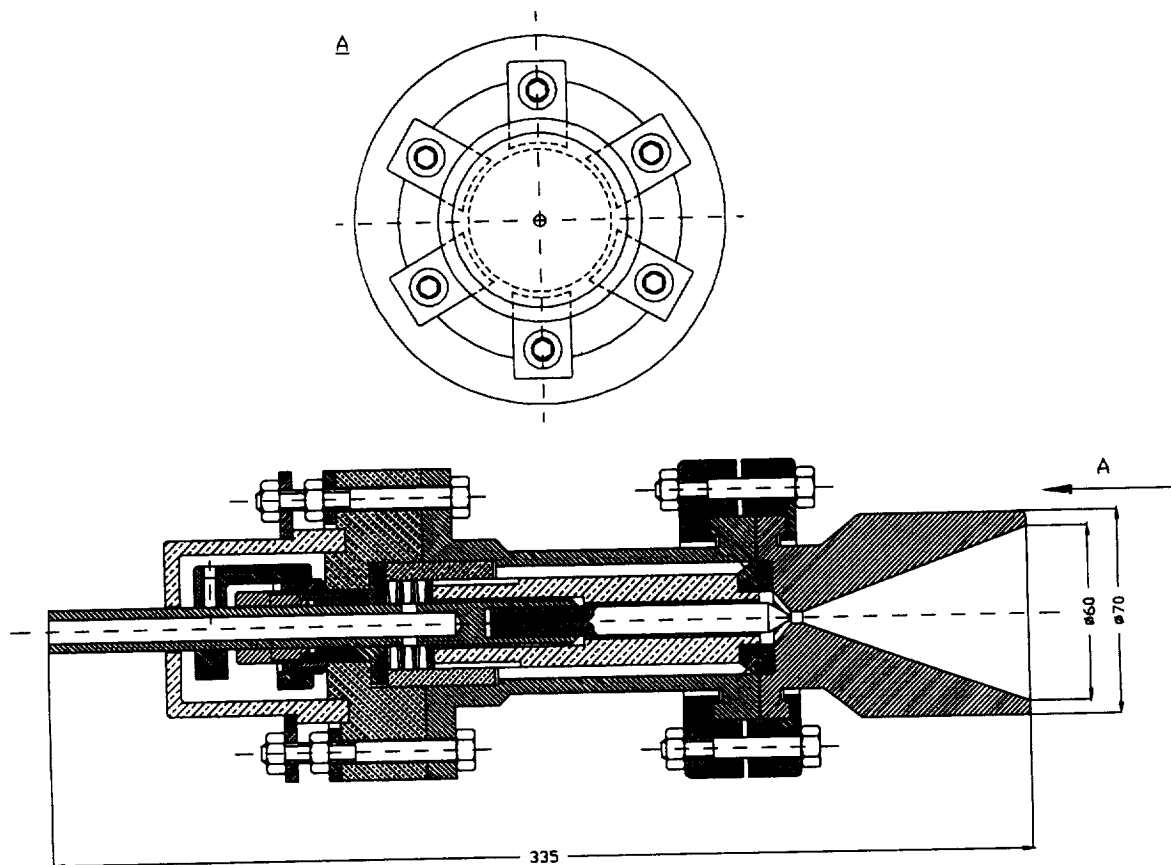


Fig. 10: Cross sectional drawing of HIPARC-R, the radiation cooled High Power Arcjet.

The thruster called HIPARC-R has a 4 mm nozzle throat diameter and a conical nozzle with an opening angle of 20°. The nozzle exit diameter is 60 mm leading to a throat to exit area ratio is 1/225. The cathode is 10 mm in diameter with a 60° cone tip. The anode nozzle body and the cathode are made of thoriated tungsten. The thruster housing, the nozzle fastening device and the propellant injector disc are made of TZM. Insulators are fabricated of boron nitride.

## References

- [1] B. Glocker, T. Rösgen, and A. Laxander: *Medium Power Arcjet Analysis and Experiments*, IEPC 91-016, 22nd International Electric Propulsion Conference, Viareggio, Italy, 1991.
- [2] J. M. Sankovic and F. M. Curran: *Arcjet Thermal Characteristics*, AIAA-91-2456, 27th Joint Propulsion Conference, Sacramento, CA, June 1991
- [3] T. M. Gölz, M. Auweter-Kurtz, H. L. Kurtz, and H. O. Schrade: *High Power Arcjet*, Third Progress Report, NASA Grant No. NAGW-1736, Institut für Raumfahrtssysteme, University of Stuttgart, Germany, February 1991

## Appendix A

Reprint of the Paper:

### High Power Arcjet Thruster Experiments

T. M. Gözl, M. Auweter-Kurtz, H. L. Kurtz, and H. O. Schrade,  
IEPC 91-072, 22nd International Electric Propulsion Conference, Viareggio, Italy, October  
1991

# Power Arcjet Thruster Experiments

T. M. Gölz, M. Auweter-Kurtz, H. L. Kurtz, and H. O. Schrade

Institut für Raumfahrtssysteme  
Universität Stuttgart

## Abstract

A water cooled laboratory model of a high power thermal arcjet was designed and built at the Institut für Raumfahrtssysteme (IRS). The thruster was designed for the 100 kW power level. It was run with hydrogen as propellant exclusively. The baseline thruster has a 6 mm throat diameter and a conical nozzle with a 20° half angle. With this thruster version a maximum specific impulse of about 1500 s was reached at an electric input power of 100 kW and a mass flow rate of 200 mg/s. Maximum input power was 140 kW with a cathode diameter of 14 mm.

The nozzle throat diameter was varied from 6 mm down to 2.5 mm, the cathode gap was varied between 2 mm and 6 mm. Data were taken over a mass flow range between 100 and 500 mg/s. The cathode shape was modified in order to find an optimal shape in terms of discharge behaviour and gas flow conditions. The current distribution in the nozzle was determined and it was found to be in good correspondence with the heat flux distribution. Furthermore, thrust and arc chamber pressure were measured.

## Introduction

Since the weight of space structures such as satellites and their lifetime have both increased in the last few years, there is a need for efficient secondary propulsion devices which provide both long lifetime and high thrust level. As the lifetime limiting factor using chemical propulsion systems is the propellant tankage, systems offering high specific impulse values are advantageous for use with such space structures.

Thermal arcjet propulsion systems offer possibilities to satisfy these demands in terms of low propellant consumption and moderate efficiency.

Most of the currently existing and former arcjet thrusters are operated in the 1-30 kW range, offering thrust levels between 0.1 and 5 N and specific impulses from 400 to 1200 s, depending on the propellant used. Best results could be achieved with hydrogen, the propellant with the lowest molar mass. Efficiencies are in the 40 % region, the best results were measured by the Giannini Scientific Corporation<sup>1</sup> in 1965 with a regeneratively cooled hydrogen arcjet in the 30 kW class. Efficiencies of 55 % and more could be reached.

In the mid sixties AVCO Corporation<sup>2</sup> had already developed and tested a hydrogen arcjet in the power level beyond 100 kW. A maximum input power of 216 kW at a specific impulse of 2210 s at a mass flow rate of 327 mg/s had been achieved.

Due to the lack of large space power systems, there has been no further research on thermal arcjets in this class until recently. As a 100 kW power source is being developed in the U.S. SP 100 program, new interest has grown in the development of high power arcjet thrusters. As a first step towards a radiation cooled thruster a water cooled thermal arcjet thruster fitting this power level has been developed at the Institut für Raumfahrtssysteme (IRS, Institute for

Space Systems). This laboratory model has been designed and built for the investigation of influences governing the performance in order to find optimum geometry for such a high power device.

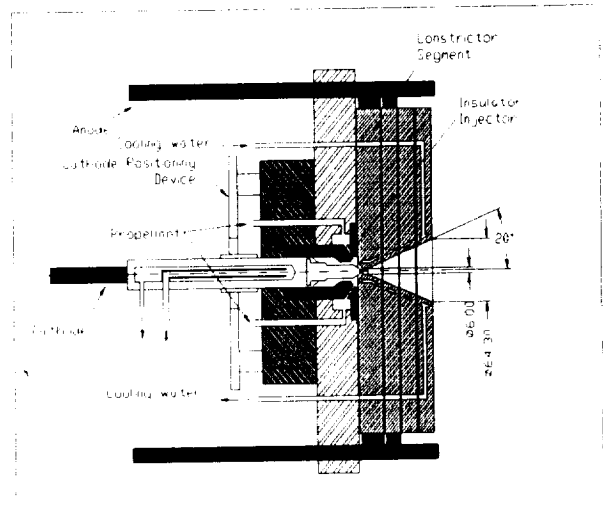


Fig. 1: Schematic Drawing of the HIPARC Thruster

## Experimental Setup

### HIPARC Thruster

HIPARC (High Power ARCjet) is a constrictor-type arcjet thruster, which consists of a stack of four individually water cooled segments, building up a conical nozzle with a 20° half angle. All nozzle segments serve as anode, where the current in each segment is measured individually. Also the heat fluxes into the cooling water of each nozzle segment and of the cathode base are determined.

The cathode is screwed on a water cooled copper tube which provides cathode base cooling. It can be moved axially in order to adjust the cathode gap.

All nozzle segments can be replaced easily, and thus a change of nozzle shape or throat diameter is easy to realize. In this paper results obtained with the four different thruster configurations given in Tab. 1 are presented.

Thruster Version	Baseline	Mod. 1	Mod. 2	Mod. 3
Throat Diameter	6 mm	2.5 mm	4 mm	4 mm
$A_E/A_t$	114:1	661:1	258:1	258:1
Constrictor l/d	1	2	1	1
Cathode Type	No. I	No. II	No. II	No. III
Mass Flow Range	100 - 500 mg/s	100 - 350 mg/s	100 - 400 mg/s	100 - 400 mg/s

Tab. 1: Thruster Configurations Tested (Cathode Types according to Fig. 3)

The propellant gas is injected through four molybdenum inserts into the arc chamber, directed 45° axially so that the jet aims into the gap between cathode tip and arc chamber wall, each of them having a tangentially directed bore hole of 0.6 mm in diameter. The four gas jets induce a swirl which stabilizes the arc by leading the plasma along the vortex train in the constrictor.

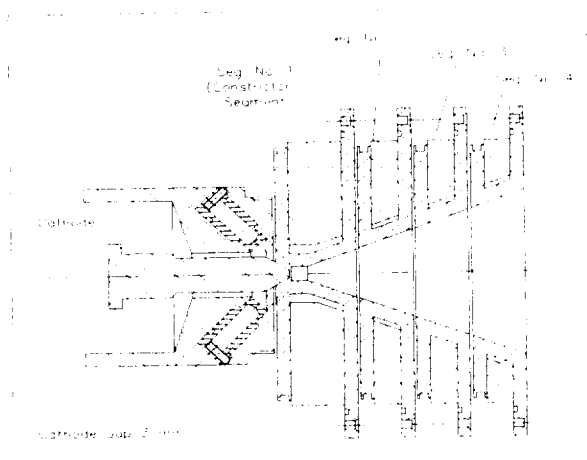


Fig. 2: Baseline Thruster Configuration

Three cathodes have been tested, two of them having a shaft diameter of 14 mm (Cathode No. I and III in Fig. 3), the third one (Cathode No. II) having a diameter of 5 mm. Cathodes No. I and III differ by their tip geometry: No. III has a 60° cone with a hemispherical tip, while No. I has a tip deepening of 2 mm radius, simulating an eroded cathode state.

### Thrust Balance

The HIPARC thruster is mounted on a thrust balance, which is an improved version of the IRS standard type<sup>3</sup>. The movable part of the balance carrying the thruster is suspended on three swing arms. Each swing arm is supported by two knife edge bearings. The thrust force is transmitted as a tension force by a thin wire over a reversing sheave to a

water cooled measuring box containing the force transducer. In order to allow the calibration of the balance under vacuum conditions, a remotely operated weight lever has been installed. This lever places a weight on a scale which creates a defined force on the platform.

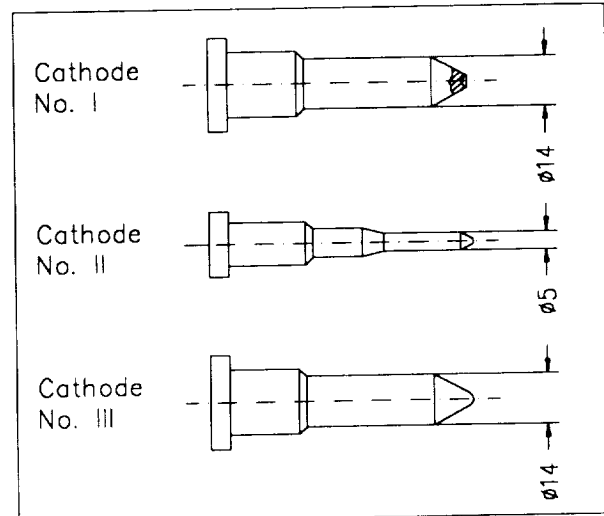


Fig. 3: Cathode Geometries Tested with HIPARC.

The electric power is fed to the thruster via two copper rods submerging into mercury filled tubes. To avoid evaporation of the mercury, its surface is sealed by silicon oil.

The cooling water for the thruster will be fed to the platform by semicircular tubes allowing minimum stiffness. Effects of stiffness and friction are calibrated for each measuring sequence before ignition and checked after engine shut down under vacuum conditions.

### Test Facilities

The HIPARC thruster and the thrust balance are integrated in a stainless steel tank of 4.5 m length and 2 m in diameter. This vacuum chamber is double walled in order to provide water cooling of the tank during thruster operation. The vacuum system, the high current supply, and the data acquisition system have been described in formerly published reports<sup>3,4</sup>.

A mass flow controller calibrated for hydrogen has been integrated into the IRS gas supply system, so that three mass flow controllers with full scale ranges of 30 slpm, 200 slpm, and 400 slpm (eq. 600 mg/s) had been available for the tests.

## Experimental Results

### General Remarks

The experiments had started with the baseline thruster version depicted in Fig. 2. This version has a 6 mm nozzle throat diameter and a cathode diameter of 14 mm with a conical tip and a tip crater (Fig. 3, Cathode No. I). At first a cathode gap of 2 mm was tested with this thruster version, including a maximum power test, where an input power of

140 kW at 1320 A with a 300 mg/s mass flow rate could be achieved<sup>5</sup>.

The current was increased until sparking occurred or when the plasma plume became unstable. It could be noticed that remarkable plume fluctuations occurred at almost the same specific power level of about 480 MJ/kg, and that cathode overheating had occurred at a current level (1320 A) where the plasma jet began to become unstable. This behaviour coincided with a voltage drop at highest current, as can be seen in the current/voltage plots in Figs. 4, 6, and 7. With the Mod. 3 thruster a maximum specific input power of about 270 MJ/kg could be achieved. Apparently the highest specific input power achievable depends on the thruster configuration, if not sparking had set the limit.

The maximum current in the following tests was set to 1000 A, or lower when sparks were observed. The sparks originated either from the constrictor wall (copper) or from the cathode tip (tungsten).

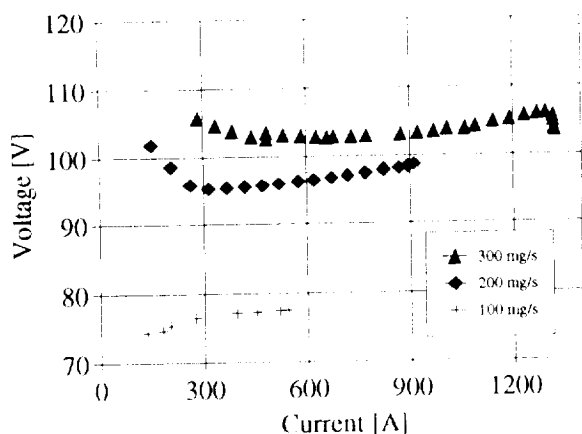


Fig. 4: Current/Voltage Characteristics obtained with the Baseline Thruster at 2 mm Cathode Gap.

The Mod. 1 thruster version (Tab. 1) had been tested next. With this thruster version it was difficult to obtain stable operation conditions. It is assumed that at low mass flow rates high arc fluctuations cause electromagnetic noise with high amplitudes, making it difficult to measure even the arc current. No reliable thrust data could be obtained at these low mass flow rates.

The Mod. 2 and Mod. 3 thruster configuration were tested subsequently. Both had a 4 mm nozzle throat; one with the 5 mm cathode diameter, the other with a 14 mm diameter and a rounded, conical tip (Fig. 3, Cathode No. III).

Copper sparks due to arc attachment in the constrictor or at the converging part of the nozzle had limited the current with the small nozzle throat. After the thruster was dismantled arc traces could be detected there.

With all cathodes used there was tungsten spitting observed beyond certain critical current levels. Where this current level was found to be at about 1320 A with cathode No. I, it is at about 500 A for cathode

No. II and for the newly machined cathode No. III. It had been observed that spitting stopped after some time, so that a further increase in current was possible up to a new critical value. With cathode type No. III this critical level could be increased to about 900 A after frequent spitting. The difference between cathode No. I and No. III is due to the difference in tip geometry: while cathode No. I has a tip deepening simulating an eroded cathode state, cathode No. III has a hemispherical tip that allows local overheating and thus sparking earlier because of the smaller tip cross section. Post test investigations of cathode No. II show a flat tip instead of the hemisphere after frequent spitting.

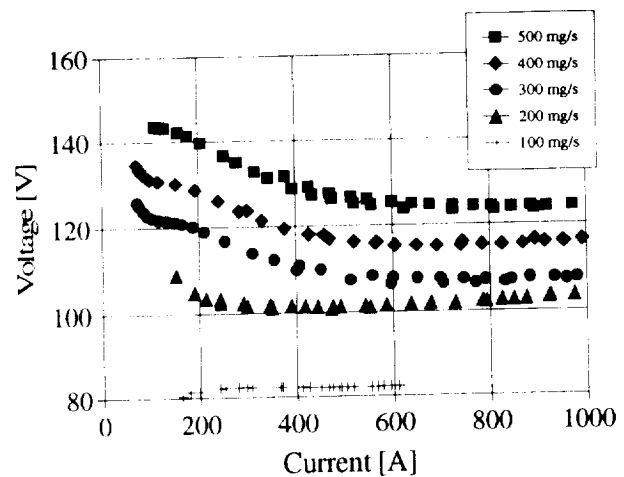


Fig. 5: Current/Voltage Characteristics obtained with the Baseline Thruster at 3 mm Cathode Gap.

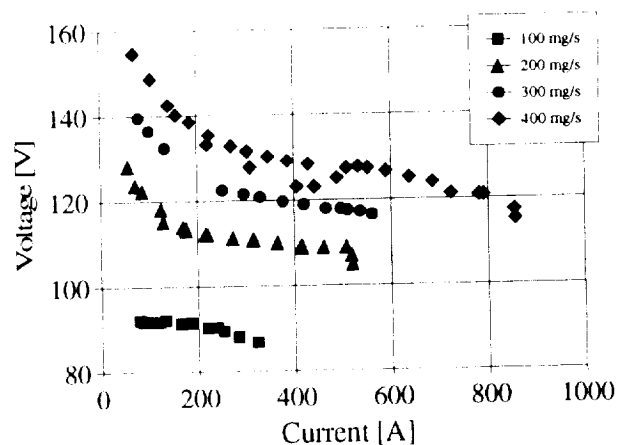


Fig. 6: Mod. 3 Thruster Version Current/Voltage Characteristics. Cathode Gap is 3 mm.

### Current/Voltage Characteristics

The arc voltage versus current characteristics show typical arcjet behaviour. An increase in current results in a decrease in voltage at low specific power levels. Figs. 4 and 5 show the curves for the baseline thruster version at 2 mm and at 3 mm cathode gap. At higher current levels the curve changes to a positive slope characteristic, which is known from MPD devices. This change in characteristics occurs at lower current at lower mass flow rates, indicating a



dependency on specific power and thus on the degree of plasma ionization.

The current/voltage characteristics for the Mod. 2 and the Mod. 3 thruster configuration were almost equal (Figs. 6, 7), except the behaviour at low mass flow rates, which can be explained by bad cathode centering that influences the characteristics mainly at low mass flow rates.

The voltage is significantly higher with smaller nozzle throat areas, with the 2.5 mm throat diameter the voltage is nearly twice the value with the 6 mm throat diameter (Figs. 5, 8).

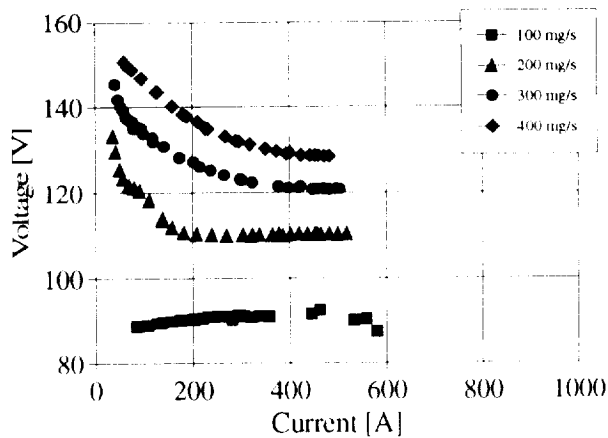


Fig. 7: Mod. 2 Thruster Version Current/Voltage Characteristics. Cathode Gap is 3 mm.

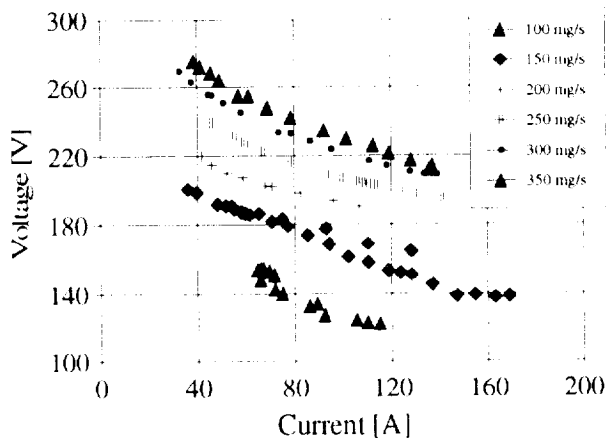


Fig. 8: Mod. 1 Thruster Version Current/Voltage Characteristics. Cathode Gap is 3 mm.

### Current Distribution

The current distribution in the anode is determined by measuring all four segment currents independently by means of shunt resistors. In order to verify these segment current measurements the sum of all segment currents is compared with the total current. In most cases the deviation is less than 1 % of the total current.

It was found that the current distribution depends on the mass flow rate, the nozzle throat diameter, the cathode size, and the total current and thus on the (specific) input power. The cathode gap was 3 mm in

all cases presented here. The segment numbering is in accordance with Fig. 2.

In Figs. 9 - 12 the current distribution in the nozzle is shown for a mass flow rate of 100 mg/s with all four thruster geometries tested. The distributions indicate that the arc attaches mainly at the constrictor segment (Segment No. 1) and at the next downstream segment, respectively.

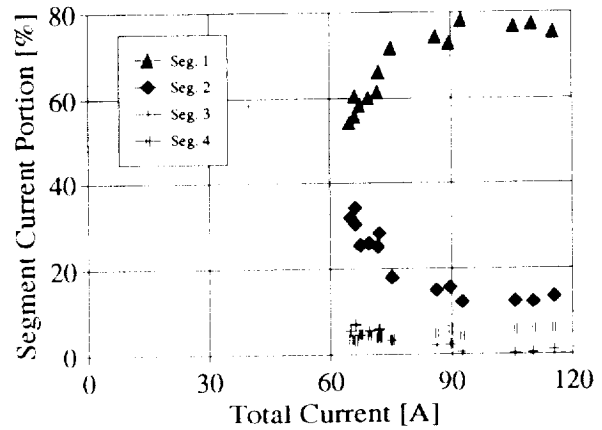


Fig. 9: Mod. 1 Thruster Version Current Distribution at 100 mg/s Mass Flow Rate.

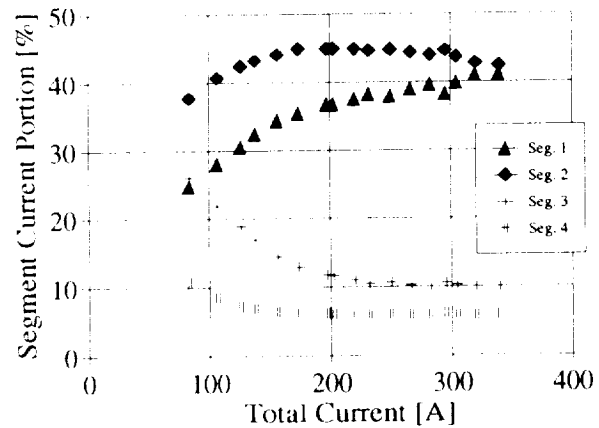


Fig. 10: Mod. 2 Thruster Version Current Distribution at 100 mg/s Mass Flow Rate.

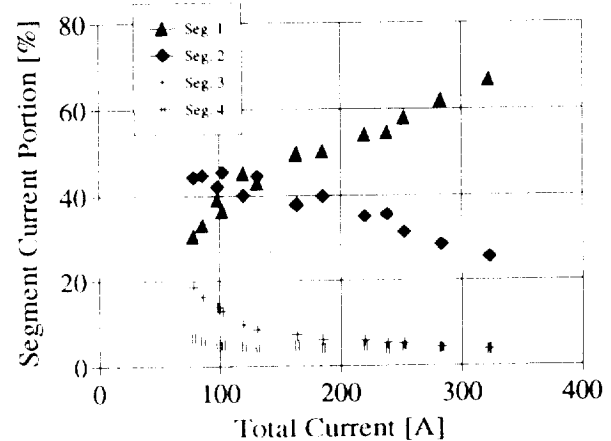


Fig. 11: Mod. 3 Thruster Version Current Distribution at 100 mg/s Mass Flow Rate.

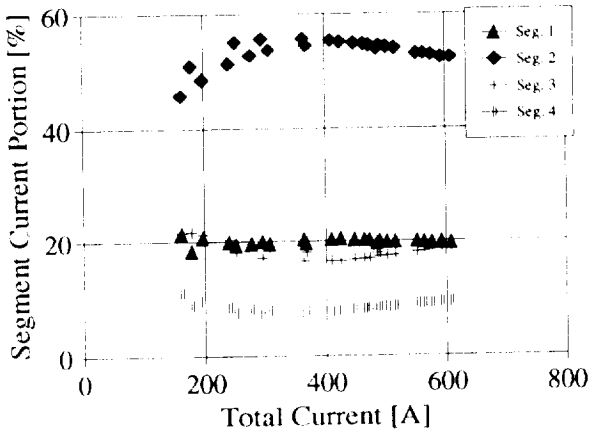


Fig. 12: Baseline Thruster Version Current Distribution at 100 mg/s Mass Flow Rate.

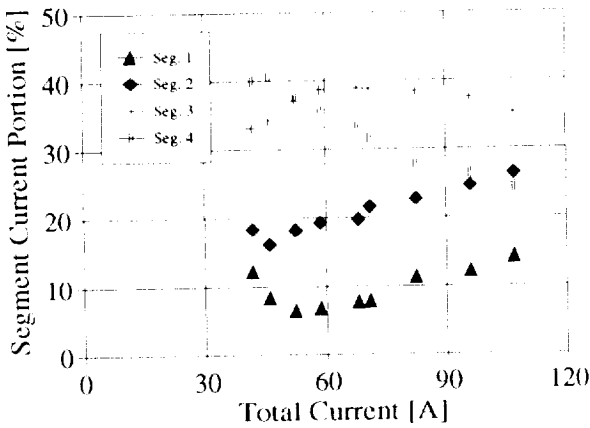


Fig. 13: Mod. 1 Thruster Version Current Distribution at 200 mg/s Mass Flow Rate.

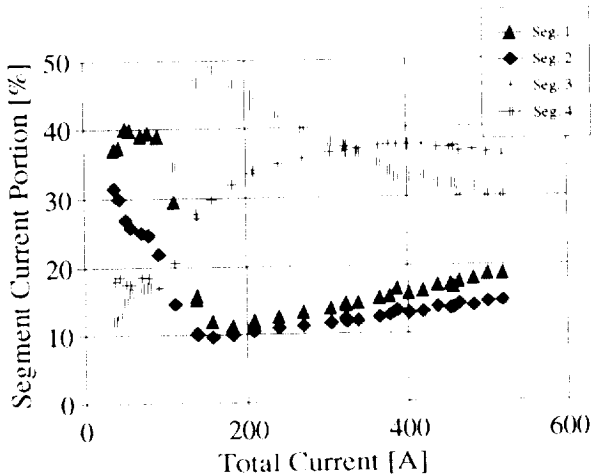


Fig. 14: Mod. 2 Thruster Version Current Distribution at 200 mg/s Mass Flow Rate.

These two segments together collect about 65 % of the total current at low current levels, increasing to between 75 % with the baseline thruster and about 90 % with the Mod. 1 and the Mod. 3 thruster at high current levels. The current portion of segment No. 3 is decreasing with higher currents, starting at between 20 and 25 % of the total current with the exception of the Mod. 1 thruster, where this segment current portion remains at levels less than 10 %. The nozzle

end segment current is not higher than 10 % with all thruster configurations tested.

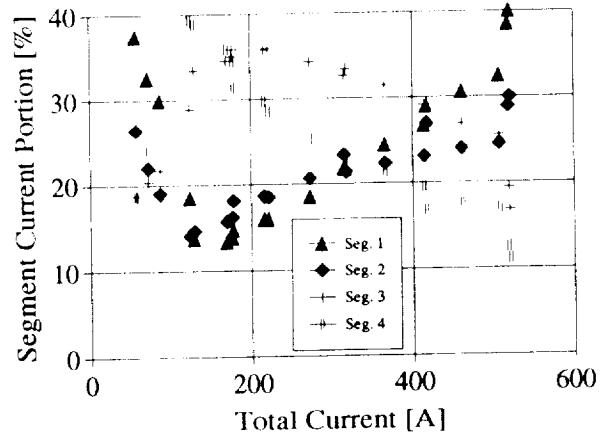


Fig. 15: Mod. 3 Thruster Version Current Distribution at 200 mg/s Mass Flow Rate.

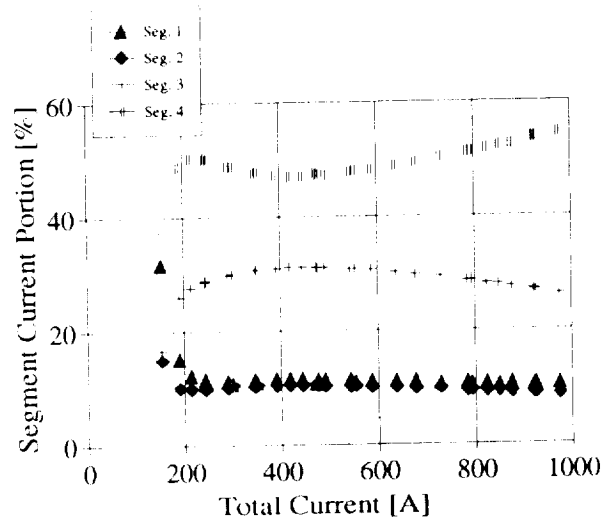


Fig. 16: Baseline Thruster Version Current Distribution at 200 mg/s Mass Flow Rate.

The current distributions obtained at a mass flow rate of 200 mg/s are depicted in Figs. 13 - 16. In a wide current range major arc attachment had occurred in the two nozzle end segments. At very low and at high current levels the arc attachment is closer to the constrictor segment. This effect is strongest with the Mod. 3 configuration (Fig. 15) and, in terms of high current behaviour, not notable with the baseline thruster (Fig. 16).

Figs. 17 - 20 show the current distributions at a mass flow rate of 300 mg/s. They show qualitatively an at least similar trend of the different segment portions with growing current. The No. 1 segment current portion develops from a lower starting level at low current to a local maximum at medium current. With the Mod. 1 (at 120 A) and the Mod. 3 thruster configuration (at 300 A) a local current portion minimum could be observed.

The segment No. 2 current portion decreases with increasing current, where a local minimum could be observed with the Mod. 3 version only.

The trend of the segment No. 3 current portion shows a decreasing behaviour with growing current with the baseline and the Mod. 2 thruster versions, and a weak dependency on the current with the two other thruster configurations.

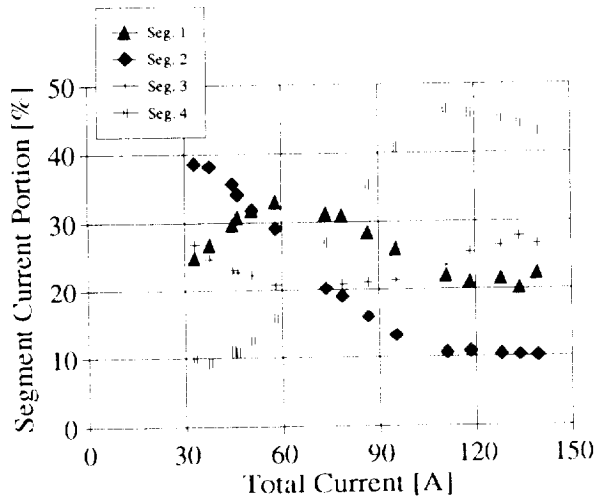


Fig. 17: Mod. 1 Thruster Version Current Distribution at 300 mg/s Mass Flow Rate.

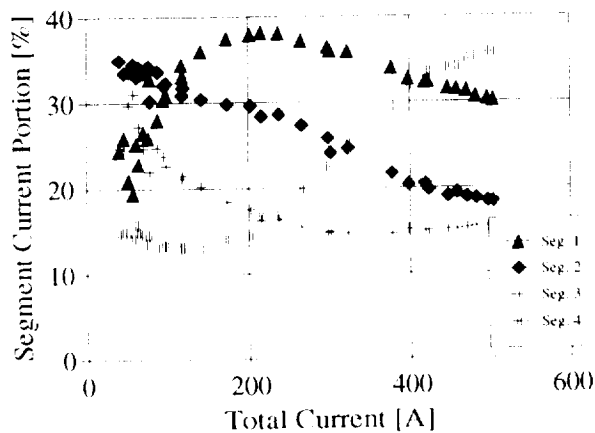


Fig. 18: Mod. 2 Thruster Version Current Distribution at 300 mg/s Mass Flow Rate.

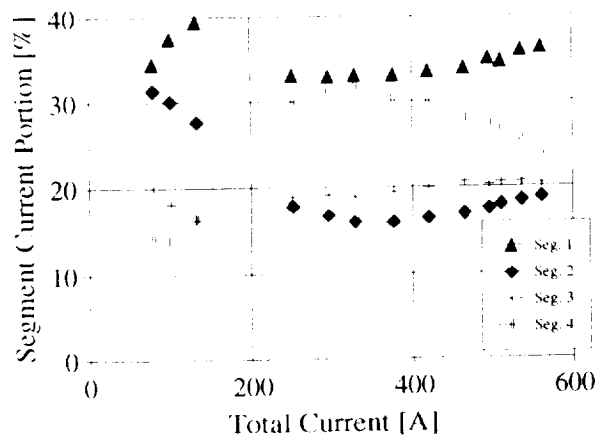


Fig. 19: Mod. 3 Thruster Version Current Distribution at 300 mg/s Mass Flow Rate.

The current portion of the nozzle end segment (Segment No. 4) starts at a value of 10 - 15 % at low current, then it decreases slightly to increase at higher current levels. With the Mod. 1 and the Mod. 3 thruster a maximum value is reached at submaximal current values. With the Baseline and the Mod. 2 thruster the trend is still increasing, but with a decreasing slope, indicating that a local maximum also could have been observed if the current had been increased to higher values.

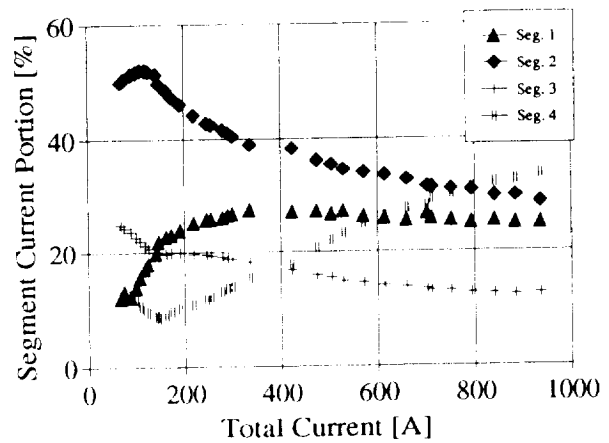


Fig. 20: Baseline Thruster Version Current Distribution at 300 mg/s Mass Flow Rate.

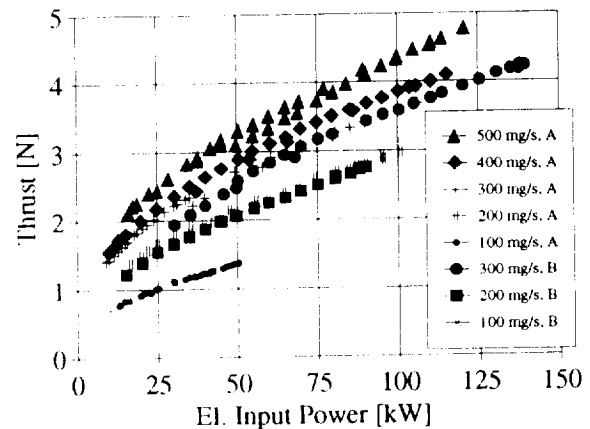


Fig. 21: Thrust versus Input Power with the Baseline Thruster Version (A: 3 mm Cathode Gap, B: 2 mm Cathode Gap).

### Performance Characteristics

All thruster versions were tested with a cathode gap of 3 mm, varying the current up to max. 1000 A and the mass flow rate in a range given in Tab. 1, with an increment of 100 mg/s for the baseline, the Mod. 2 and the Mod. 3 thruster versions, and 50 mg/s with the Mod. 1 thruster version.

With the baseline thruster version the highest specific power values and thus the best specific impulse values could be realized. Fig. 21 shows the thrust versus input power characteristics for all five mass flow rates tested; specific values are depicted in Fig. 22. The highest specific power was 500 MJ/kg, where a specific impulse of 1520 s could be reached

with the 200 mg/s mass flow rate. Higher power levels could not be achieved at this mass flow rate due to unstable jet behaviour.

Fig. 23 shows a zoomed section of Fig. 22. Best specific impulses at a given specific power were achieved at a mass flow rate of 200 mg/s.

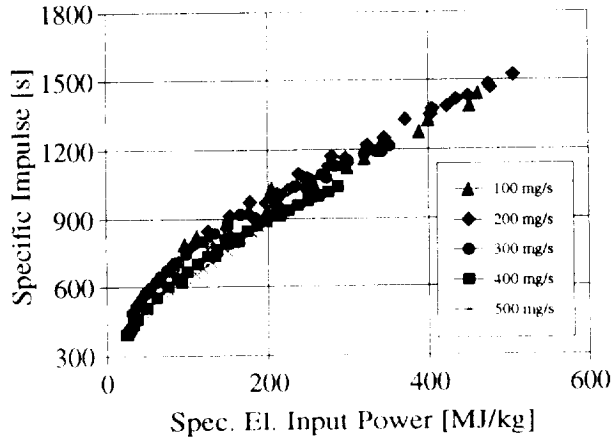


Fig. 22: Specific Impulse versus Specific Input Power with the Baseline Thruster Version.

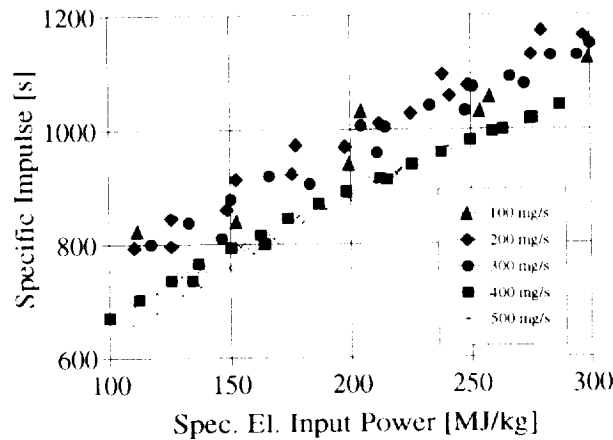


Fig. 23: A more detailed View of Specific Impulse versus Specific Input Power with the Baseline Thruster Version.

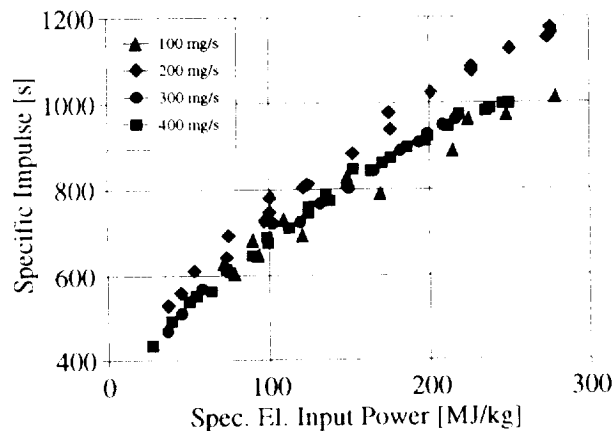


Fig. 24: Specific Impulse versus Specific Input Power with the Mod. 3 Thruster Version.

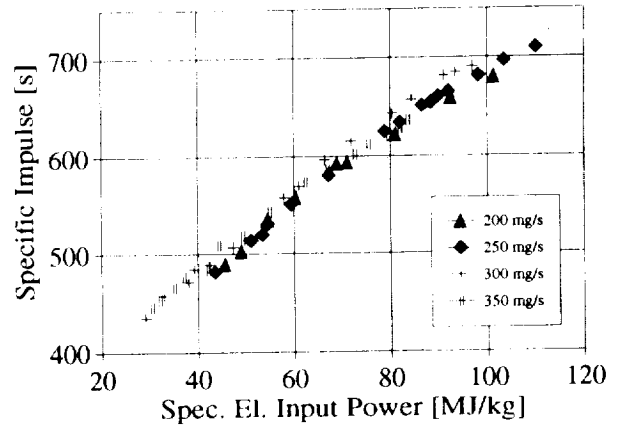


Fig. 25: Specific Impulse versus Specific Input Power with the Mod. 1 Thruster Version.

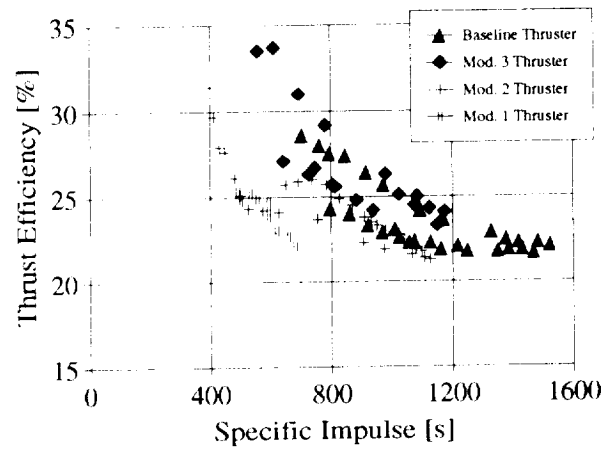


Fig. 26: Efficiency versus Specific Impulse at 200 mg/s Mass Flow Rate.

Errors in the thrust measurement due to thermal drifting effects could not be avoided completely, their magnitude was negligible at the 100 mg/s mass flow rate and could be kept smaller than 0.1 N at the other mass flow rates, so that the resulting error in specific impulse did not exceed 50 s at 200 mg/s mass flow rate. A maximum specific impulse value of  $1520 \text{ s} \pm 50 \text{ s}$  was achieved with a mass flow rate of 200 mg/s at the 100 kW power level, which was the upper power limit for this mass flow rate because of cathode spitting. With 100 mg/s mass flow rate the input power was limited to 50 kW due to cathode spitting; a specific impulse value of 1400 s could not be exceeded.

The thrust efficiency is defined as the quotient of total thrust power divided by the electric input power:

$$\eta_T = \frac{F^2}{2 \dot{m} U I}$$

The thrust efficiency decreases with increasing specific impulse, which is a consequence of growing particle excitation energies, which cannot be fully recovered in the expansion nozzle. The thrust efficiency versus specific impulse characteristic at a mass flow rate of 200 mg/s for all four thruster versions tested is depicted in Fig. 26. The efficiency at

maximum specific impulse was 22 % with the 6 mm nozzle throat.

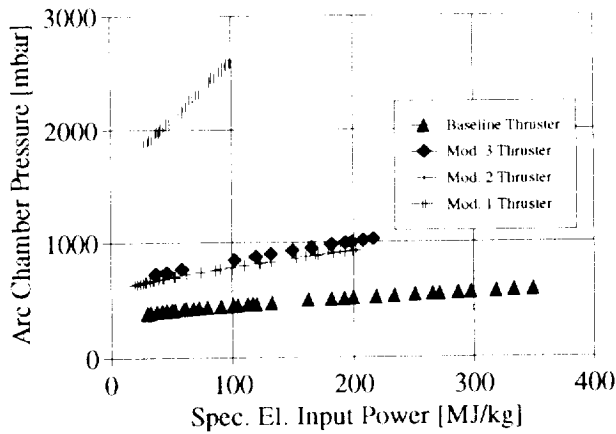


Fig. 27: Arc Chamber Pressure versus Specific Input Power at 300 mg/s Mass Flow Rate.

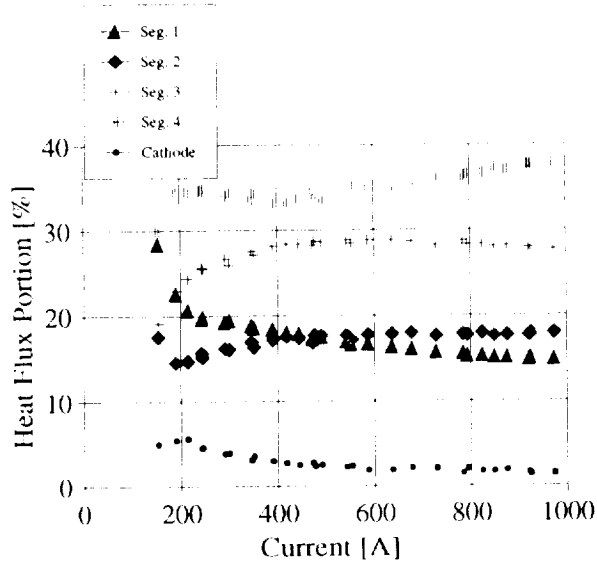


Fig. 28: Heat Flux Distribution in the Anode with the Baseline Thruster at 200 mg/s Mass Flow Rate.

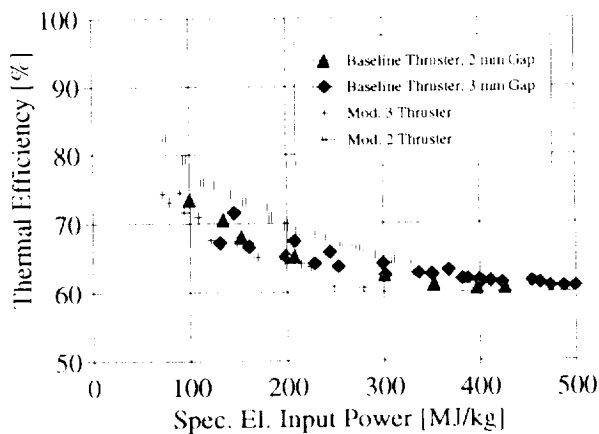


Fig. 29: Thermal Efficiency Characteristics at 100 mg/s Mass Flow Rate.

### Arc Chamber Pressure Characteristics

The arc chamber pressure depends on the nozzle throat diameter and on the mass flow rate, and it increases monotonously with increasing input power. The highest pressure value of 2.9 bar could be obtained at a maximum power of 30 kW with the smallest nozzle throat (2.5 mm) and the highest mass flow rate (350 mg/s). Higher mass flow rates could not be realized with this thruster version, because the supply pressure limit was reached.

The arc chamber pressure is also influenced by the cathode gap and the cathode size. With the big nozzle throat three different cathode gaps were tested, and with the Mod. 2 and Mod. 3 thruster versions cathode diameters of 5 mm and 14 mm were investigated.

Due to the variation of arc chamber volume by changing the cathode size, there is an increase in chamber pressure with the bigger cathode. Fig. 27 illustrates the dependency of the arc chamber pressure on throat diameter and on cathode size at a mass flow rate of 300 mg/s.

### Heat Flux Measurements

The dimensions of a radiation cooled thruster mainly depend on the amount of heat that has to be radiated to the surrounding space. In order to determine this amount of heat, the heat flux into the anode segment and cathode cooling water was calculated by measuring the segment cooling water mass flow rate and the water temperature before entering and after leaving the thruster.

The heat flux distribution was found to be in good correlation with the current distribution in the anode. Fig. 28 shows the heat flux distribution in the baseline thruster version at a mass flow rate of 200 mg/s. Comparing this figure with the current distribution obtained at the same time (Fig. 16), it can be stated that the distributions are qualitatively the same, but that there are differences in the quantities.

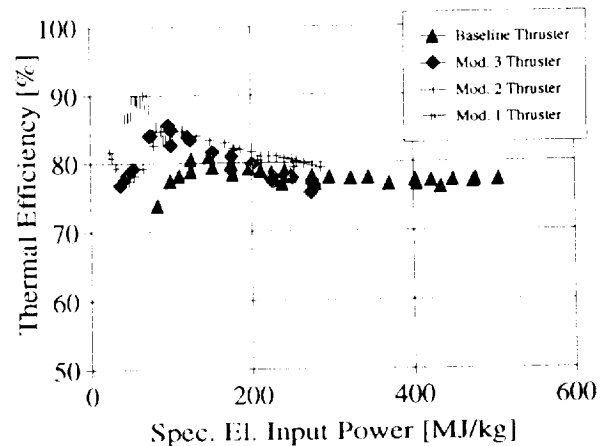


Fig. 30: Thermal Efficiency Characteristics at 200 mg/s Mass Flow Rate.

The thermal efficiency  $\eta_{th}$  yields the portion of the input power which remains in the gas after subtracting the heat flux power transferred to the cooling water. The definition is

$$\eta_{th} = \frac{P_{el} - \dot{Q}_{total}}{P_{el}}$$

with  $P_{el}$  being the electric input power, and  $\dot{Q}_{total}$  being the sum of all segment heat fluxes, including cathode base cooling. The results show a decrease of thermal efficiency with increasing input power, and an increase in thermal efficiency with increasing mass flow rate. The biggest effect could be noticed between the 100 mg/s and the 200 mg/s mass flow rate, as it is depicted in Figs. 29 and 30. Although a further increase in mass flow rate can be noticed in a further rise of thermal efficiency, this effect is rather insignificant (Fig. 31).

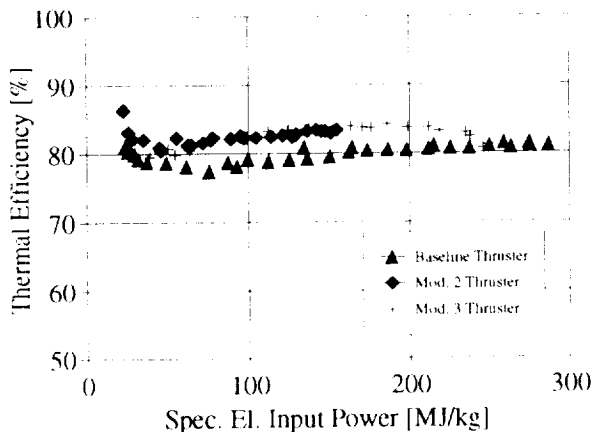


Fig. 31: Thermal Efficiency Characteristics at 400 mg/s Mass Flow Rate.

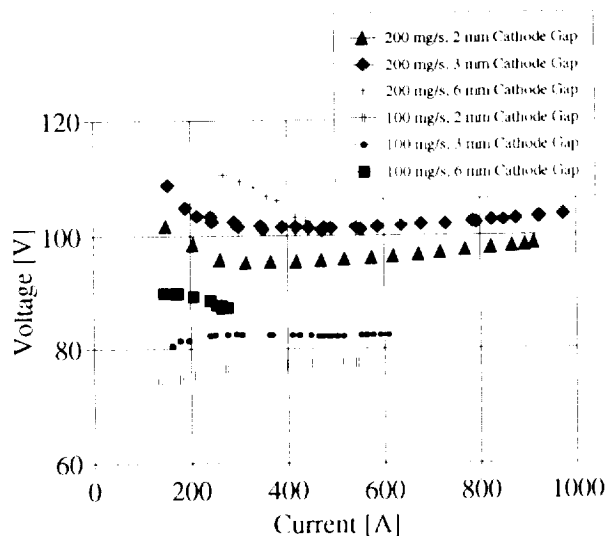


Fig. 32: Current Voltage Characteristics at Different Cathode Gaps obtained with the Baseline Thruster Version.

### Influence of the Cathode Gap

With the 6 mm throat diameter cathode gaps of 2 mm, 3 mm, and 6 mm were investigated.

The effect on current/voltage characteristics can be seen in Fig. 32. It shows a direct dependency of the arc voltage on the cathode gap up to a certain critical cathode gap. As a reason it is assumed that the arc length cannot exceed a certain critical value burning stable, and that in the unstable mode the arc attachment is in the converging part of the constrictor segment or in the constrictor itself.

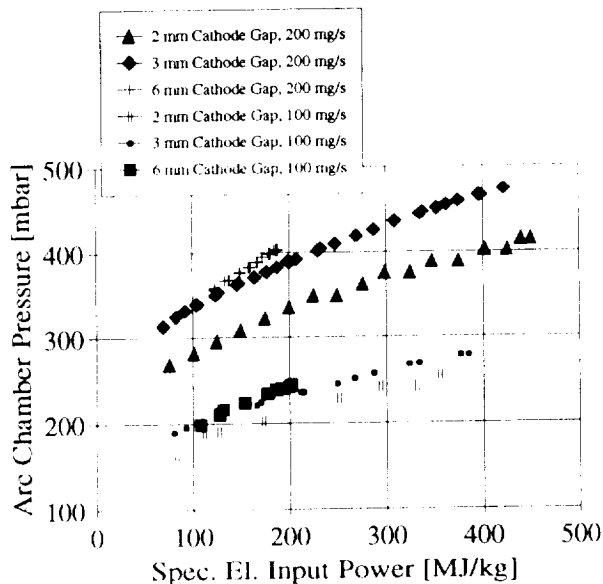


Fig. 33: Dependency of the Arc Chamber Pressure from the Cathode Gap with at 6 mm Nozzle Throat.

A direct consequence of the higher voltage level is the increased input power at a given current value at higher cathode gaps, which increases the maximum specific power at a given (maximum) current. Or, from another point of view, the thermal load on the cathode was decreased with bigger cathode gap at a given specific input power. As an example, with the baseline thruster maximum specific input levels of 470 MJ/kg could be realized with the 2 mm cathode gap, whereas the maximum specific input power was 500 MJ/kg with a cathode gap of 3 mm. Higher specific input powers yield higher specific impulses.

Another effect was observed on the arc chamber pressure, which is the higher the more the cathode is moved away from the constrictor (Fig. 33). This can be explained by the longer arc column at bigger cathode gap, which means more ohmic heating in the arc chamber and thus higher arc chamber temperature and pressure.

No effect on specific impulse or efficiency could be stated; Fig 34 shows the specific impulse versus specific power characteristics for all three cases.

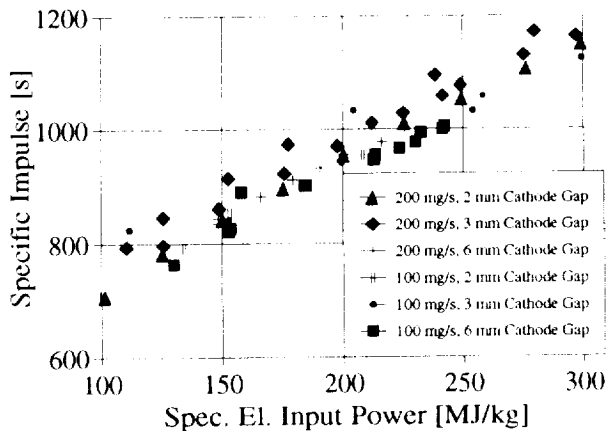


Fig. 34: Specific Impulse versus Specific Input Power for Different Cathode Gaps obtained with the Baseline Thruster Version.

### Influence of the Nozzle Throat Diameter

As already mentioned above, the nozzle throat diameter did not directly influence the performance characteristics of HIPARC. A strong influence was noticed only on the maximum power levels that could be reached, which were the highest with the largest nozzle throat. The heat load to the constrictor seems to be the power limiting factor.

As already mentioned above, arc voltage and arc chamber pressure vary inversely with the nozzle throat diameter, but these parameters did not effect the performance characteristics.

### Conclusions and Discussion

The HIPARC thruster was tested with a variety of 3 nozzle throat diameters, several different mass flow rates, with three different cathode shapes and at three different cathode gaps.

The mass flow rate was found to have a major influence on thruster performance. There seems to be an optimum mass flow rate at about 200 mg/s, where more than 1500 s of specific impulse could be obtained and where the efficiency reaches 22 %. Although these thrust efficiencies are only moderate, they agree very well with the theoretically predicted values. The maximum total thrust efficiency possible is given as

$$\eta_{\text{total}} \approx \eta_{\text{thermal}} \eta_{\text{frozen}}$$

where the thermal efficiency is between 60 % and 80 % with the water cooled thruster presented here, and the frozen flow efficiency at an arc chamber pressure of 1 bar and specific impulse values around 1500 s is about 30 % with hydrogen. Thus a maximum efficiency of 24 % cannot be exceeded at these high specific impulse values.

The thermal efficiency will improve by changing the cooling concept of the thruster to radiation cooling, mainly because of the amount of heat radiated from the walls back to the propellant gas. This effect is more pronounced for higher chamber

pressures. On the other hand, the frozen flow efficiency decreases with increasing chamber pressure.

Specific impulses mainly depend on the specific input power; higher values than achieved seem to be possible with the baseline thruster version at higher current levels with the 3 mm cathode gap, where the limit was not yet reached. Nevertheless, the maximum values in specific input power of 500 MJ/kg achieved here with the water cooled device yield specific impulse values beyond the 2000 s limit with a radiation cooled HIPARC<sup>6,7</sup>.

It is difficult to draw a conclusion for the design of a radiation cooled arcjet thruster, the result depending on the design goal. High specific impulses require high specific input powers and thus large nozzle throat diameters yielding low arc chamber pressures, whereas higher efficiencies require high arc chamber pressures and thus smaller nozzle throats, which prohibit high specific powers.

### Acknowledgement

The work on the high power arcjet HIPARC is supported by NASA Grant No. NAGW-1736. This support is greatly appreciated.

### References

- [1] J. P. Todd: "Thirty kW Arc Jet Thruster Research", Rep. No. FR024-10338 (APL-TDR-64-58), Giannini Electric Co., August 1964
- [2] AVCO Research Corporation: "Thirty Kilowatt Plasma Rocket Engine Development, Third Year Development Program", Summary Report, RAD TR-64-6 NASA CR-54044, July 1964
- [3] H. L. Kurtz, M. Auweter-Kurtz, B. Glocker, W. Merke, H. O. Schrade: "A 15 kW Experimental Arcjet", IEPC 88-107, 20th Int. Electric Propulsion Conference, Garmisch-Partenkirchen, FRG, 1988
- [4] B. Glocker, M. Auweter-Kurtz, T. M. Gözl, H. L. Kurtz, H. O. Schrade: "Medium Power Arcjet Thruster Experiments", AIAA 90-2531, Institut für Raumfahrtssysteme, Universität Stuttgart, Germany, 1990
- [5] T. M. Gözl, M. Auweter-Kurtz, H. L. Kurtz, H. O. Schrade: "High Power Arcjet", Third Progress Report IRS 91-P3 for NASA Grant No. NAGW-1736, Stuttgart, Germany, 1991
- [6] B. Glocker, T. Rösger, A. Laxander: "Medium Power Arcjet Analysis and Experiments", IEPC 91-016, 22nd Int. Electric Propulsion Conference, Viareggio, Italy, 1991
- [7] T. Haag and F. M. Curran: "High Power Hydrogen Arcjet Performance", AIAA-91-2226, 27th Joint Propulsion Conference, Sacramento, CA, 1991

